Design of a multi-energy hard x-ray camera for profile measurements at WEST tokamak

T. Barbui[1], L. F. Delgado-Aparicio[1], Y. Peysson[2], B. Stratton[1], O. Chellaï[1], K. Hill[1], N. Pablant[1]

[1] *Princeton Plasma Physics Laboratory, Princeton, NJ 08540, USA*

[2] *CEA, IRFM, 13108 Saint-Paul-lez-Durance, France*

The WEST tokamak is currently being prepared for long pulse operation with a water-cooled full tungsten divertor. Heating will be provided by radiofrequency systems, including lower hybrid current drive (LHCD). When electron heating is done by LH waves, temperature measurements carried out with the Electron Cyclotron Emission (ECE) diagnostic are challenging because ECE radiation temperature and plasma temperature are different. However, hard x-ray (HXR) temperature measurements during the LHCD pulse are possible. The HXR emission can also be used to investigate the non-thermal tail of the electron distribution function, which is crucial for estimating the efficiency of the LHCD and the birth of runaway electrons. In this context the Princeton Plasma Physics Laboratory has designed and built a compact multi-energy hard x-ray camera (ME-HXR) for time, space and energy-resolved measurements of the electron temperature, the fast electron tail density produced by LHCD and runaway electrons, and the beam-target emission of tungsten at the edge due to fast electron losses interacting with the metal target.

The HXR detector and his energy configuration settings

The ME-HXR camera employs a 2D pixelated x-ray detector produced by DECTRIS [1]. The detector is a PILATUS3 X 100K-M CdTe single-photon counting detector that has high quantum efficiency (>50%) up to ~100 keV x-ray energy. The CdTe sensor consists of a continuous array of 487 × 195 = ~100k pixels covering an active area of 33.5 mm × 83.8 mm. Pixel size is 172 μm. This detector has the great advantage of allowing the lower energy threshold to be set independently for each pixel, in order to measure the x-ray emission with spatial, temporal and energy resolution simultaneously. The energy dependence of each pixel was calibrated for different energy intervals within the range 8-100 keV with a resolution that varies from 1.5 keV at low energy to 20 keV at high energy [2]. The energy subdivision of the detector can be set by using different configurations according to the physics goal. Pixels along the columns or rows of the detector can be set to have the same energy threshold, to allow spatial resolution along one direction and energy along the other. One possible energy

subdivision is depicted in Figure 1(b) having the pixel columns to the same energy and have spatial resolution along the rows of the detector. Another configuration depicted in Figure 1(c) is based on setting an entire row to the same energy value and repeating the energy subdivisions along the rows of the detector. The spatial resolution of the diagnostic depends on the chosen pixel configuration besides the geometry. The first configuration gives a high spatial resolution of 14 mm. The second configuration gives a lower spatial resolution of ~ 4 cm. The temporal resolution is limited by the detector maximum frame rate to 2 ms.

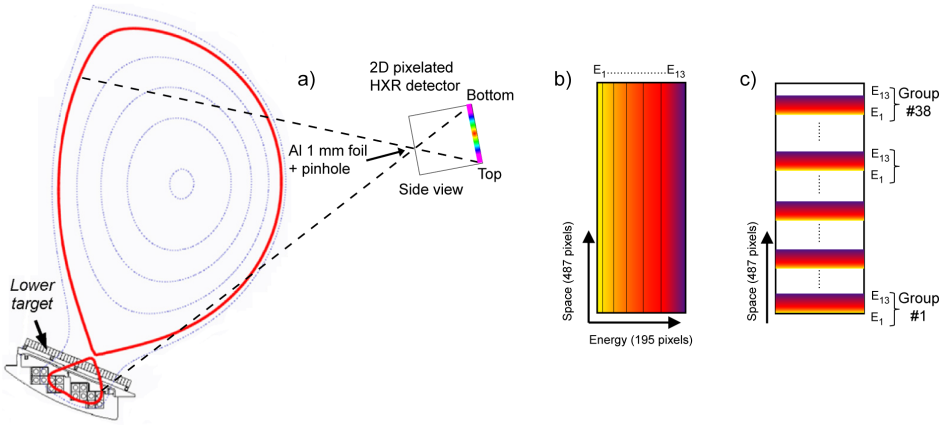

Figure 1. (a) Detector setup showing WEST cross-section. (b) Horizontal arrangement of energy thresholds (c) Vertical arrangement of energy thresholds.

The ME-HXR aims at measuring different physical quantities and the energy configuration of the pixels will be set accordingly:

1. T_e profile: sampling the low-energy continuum from 12 to 30 keV and filtering out the W line emission at $E < 12$ keV. Energy subdivision of the detector will be between 12 and 30 keV with 3 keV increments.
2. $n_{e,fast}$ profile: sampling the non-thermal emission from fast-e induced by LHCD at $E >$ 20 keV. Energy subdivision of the detector will be between 30 and 100 keV with 10 keV increments.
3. Beam-target reactions: K emission of tungsten at the edge due to fast electron losses interacting with the metal target ($K_\alpha = 59$ keV, $K_\beta = 67$ keV). Energy subdivision of the detector will be between 30 and 80 keV with 6 keV increments.

Diagnostic design

The schematic of the diagnostic assembly is shown in Figure 2, and its main components are labeled. The detector is placed inside a stainless steel tube which is mounted on an upper radial port on WEST. Vacuum window consists of a 1 mm Al window which has the twofold function of vacuum interface and blocking W line radiation at $E < 10$ keV. The tube will be pumped down to the mTorr level to maintain a low level of humidity required for the detector operation

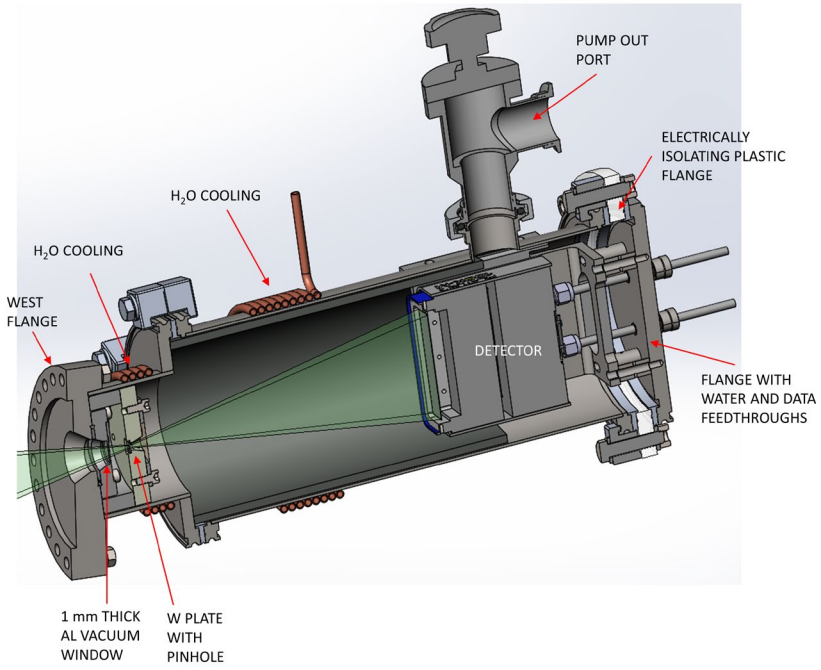

Figure 2. ME-HXR assembly with the main components labelled.

and to protect the WEST vacuum vessel in case of a failure of the vacuum window. The field of view is determined by a pinhole geometry. A horizontal slit of dimensions 4 × 1 mm is obtained by machining a tungsten plate positioned after the vacuum window. The slit height defines the vertical extension of the field of view (93 cm) which covers most of the WEST cross section including the lower divertor (see Figure 1(a)).

Modelling of a WEST discharge with LHCD

A WEST discharge with LHCD was modelled with the suite of codes C3PO/LUKE/R5-X2. C3PO is a ray tracing code that models the LH wave transmission and absorption in the plasma [3]. LUKE is a bounce-averaged relativistic Fokker–Planck solver, which calculates the electron distribution function [4]. R5-X2 is a quantum relativistic bremsstrahlung code which computes the non-thermal bremsstrahlung emission from fast electrons during LHCD [5]. The ME-HXR geometry has been incorporated in R5-X2 to allow creation of synthetic line-integrated HXR profiles. The simulated discharge is #55550 (t = 5.5 s) with a total of P_{LH} = 3.3 MW divided into two rays. Ray#1: P_{LH} = 2.33 MW, $n_{\parallel}$ = -1.97; ray#2: P_{LH} = 1 MW, $n_{\parallel}$ = 6. T_{e0} = 5.3 keV, n_{e0} = 3.8×10^{19} m^{-3}. The results of the LH modelling with the power deposition and current profiles are shown in Figure 3(a-b). The LH wave is absorbed almost entirely off axis. The first ray has the absorption peak at ρ=0.4 and drives co-current. The second ray has the absorption peak at ρ=0.8 and drives a small counter-current. The line-integrated HXR profiles determined using the ME-HXR sightline geometry are shown in Figure 3(c). At lower energies (<20 keV), the profiles are centrally peaked due to the dominant contribution of thermal emission. At higher energies, non-thermal emission induced by LH creates two symmetric shoulders at the location where LH power is mainly absorbed (chords 11 and 38 corresponding

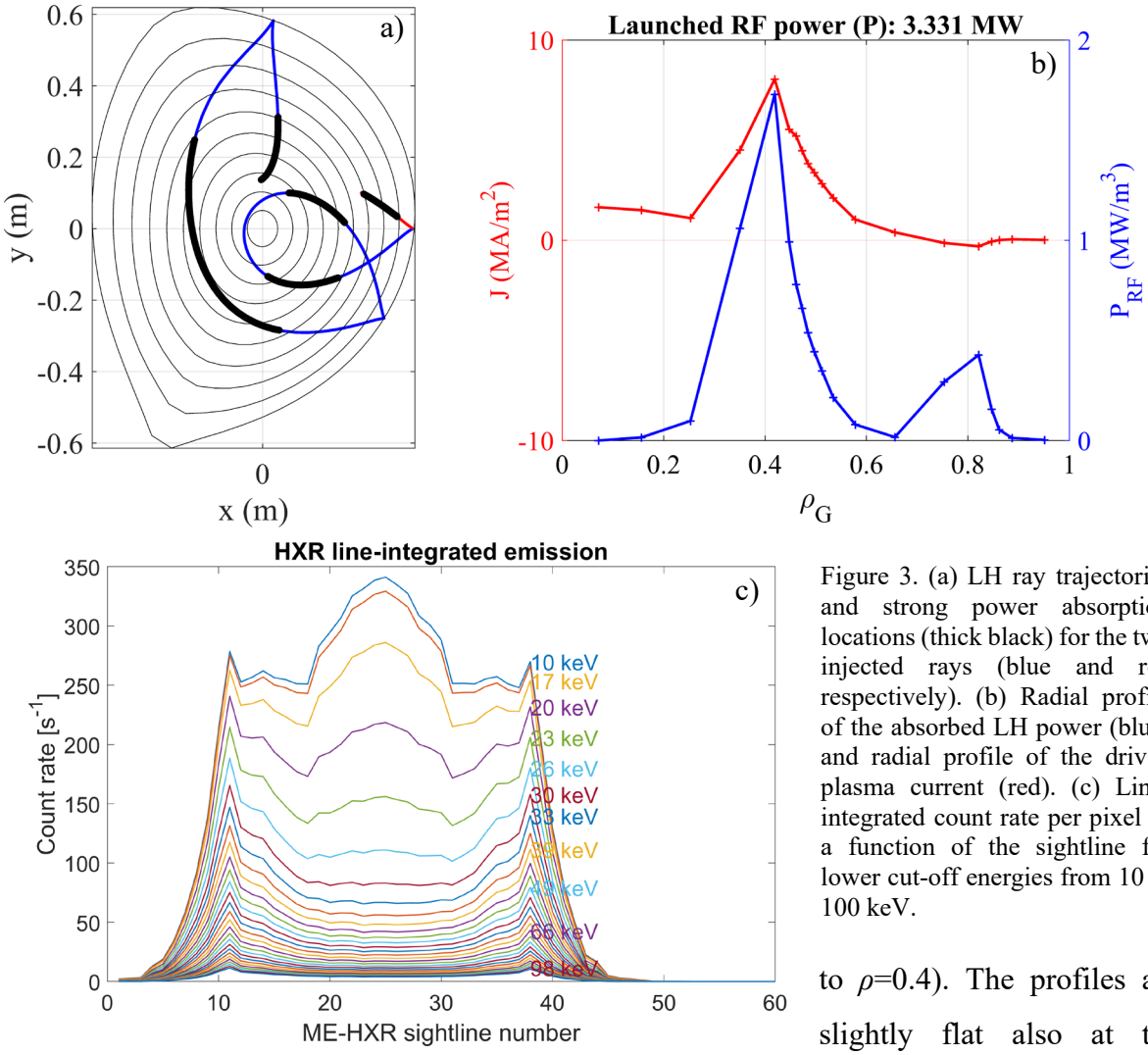

Figure 3. (a) LH ray trajectories and strong power absorption locations (thick black) for the two injected rays (blue and red respectively). (b) Radial profile of the absorbed LH power (blue) and radial profile of the driven plasma current (red). (c) Line-integrated count rate per pixel as a function of the sightline for lower cut-off energies from 10 to 100 keV.

to ρ=0.4). The profiles are slightly flat also at the location of the second absorption peak (chords 5 and 43 corresponding to ρ=0.8). Chords 50-60 cover the lower divertor and therefore see no signal in the LH modelling but they are useful for measuring beam-target reactions. This modelling suggests that a time integration of ≥ 20 ms is needed to have sufficient signal on the detector up to an energy threshold of 100 keV (using the configuration in Figure 1(c) and binning row pixels).

References

[1] "DECTRIS Ltd.," [Online]. Available: www.dectris.com.

[2] T. Barbui, L. F. Delgado-Aparicio, N. Pablant, Disch, C. Luethi, N. Pilet, C., B. Stratton and P. VanMeter, *Rev. Sci. Instrum.,* vol. 92, p. 023105, 2021.

[3] Y. Peysson, J. Decker and L. Morini, *Plasma Phys. Control. Fusion,* vol. 54, p. 045003, 2012.

[4] Y. Peysson and J. Decker, *Fusion Sci. Technol.,* vol. 65, p. 22, 2014.

[5] Y. Peysson and J. Decker, *Phys. Plasmas,* vol. 15, p. 092509, 2008.

Acknowledgements

This work is supported by the U.S. DOE-OFES under Contract No. DE-AC02-09CH11466.